Large Deflection Behavior of Circular Quasi-Isotropic Laminates Under Point Loading

Ajit Kelkar*
North Carolina A&T State University, Greensboro, North Carolina
W. Elber†
NASA Langley Research Center, Hampton, Virginia
and
I. S. Raju‡
Analytical Services and Materials Inc., Hampton, Virginia

Eight-ply quasi-isotropic circular composite plates of Thornel 300 graphite in Narmco 5208 epoxy resin (T300/5208) were analyzed to obtain the large deformation behavior under low-velocity impact-type point loads. A simple plate-membrane coupling model was developed. The impact-type point loads were replaced by equivalent quasistatic point loads. The plate-membrane coupling model was used to obtain the large deformation shapes for the thin circular composite laminates. The analyses indicated that the large deformation shapes of the composite plates under point loads vary with the center point displacements, and hence are different for different load levels. Quasi-isotropic plates were analyzed by replacing anisotropic bending stiffness components with the equivalent flexural stiffness for the isotropic plates. The plate-membrane coupling model was verified by conducting a series of tests on clamped, circular quasi-isotropic laminates. Deflected shapes and load-displacement curves for the thin composite plates were experimentally obtained. These deflected shapes and load-displacement curves agreed well with the analytical results obtained using the plate-membrane coupling model.

Nomenclature

a = radius of the plate or membrane
A = extensional stiffness matrix
B = coupling stiffness matrix
D = bending stiffness matrix
D_{eq} = equivalent bending stiffness
E = Young's modulus
E_{eq} = equivalent Young's modulus
E_{11} = lamina Young's modulus in fiber direction
E_{22} = lamina Young's modulus perpendicular to the fiber direction
G_{12} = lamina shear modulus
h = thickness of the plate or membrane
κ = curvature
M = bending moment
$p(r)$ = pressure at any radius r
P = point load
r,θ,z = cylindrical coordinate system
u = radial displacement
U_b = strain energy due to bending
w = transverse displacement
w_0 = transverse displacement at the center of the plate
σ_r = radial stress (membrane)
ν_{eq} = equivalent Poisson's ratio
ξ = dummy variable

Received March 14, 1985; presented as Paper 85-0723 at the AIAA/ASME/ASCE/AHS 26th Structures, Structural Dynamics and Materials Conference, Orlando, FL, April 15-17, 1985; revision received April 10, 1986.

*Assistant Professor.
†Head, Fatigue and Fracture Branch, Materials Division.
‡Senior Scientist. Member AIAA.

N.B. Use of trade names or manufacturers does not constitute an official endorsement, either expressed or implied, by the National Aeronautics and Space Administration.

Introduction

GRAPHITE fiber composite laminates can have significantly higher strength-to-density ratios than aluminum alloys. But they have low-ultimate strains, no plastic deformation range, and no useable strength in the thickness direction. These limitations are obvious when the laminates are impacted by tools, hail, or other hard objects. Any internal matrix damage, even if invisible from the surface, lowers the compressive strength of the composite laminates. To improve the material performance in impact requires a better understanding of the deformation and damage mechanics under impact-type loading.

Impact events can be characterized in three velocity domains: Ballistic impact, representative of hostile projectile or bullet impact, considered a local phenomenon; flight velocity impacts, represented by bird strikes or runway debris impacts, involving the dynamic response of the local structure; and low-velocity impacts, represented by handling damage such as dropping tools, footsteps, and similar events. In many cases, the low-velocity problem primarily involves the basic first mode of structural deformation.

The low-velocity impact is simpler to analyze because, in many cases, the deformation mechanics can be represented by static deformation mechanics. Llorens and Gause[1] were the first to analyze the impact problem with a linear plate bending theory and to perform quasistatic impact tests. Bostaph and Elber[2] followed the same approach but recognized that large deformation theory, as well as the addition of plate shear deformations, were required to describe the deformation behavior of thin laminates in the undamaged state. They used a superposition approach to match the plate bending solution and a membrane solution under the

load points, thus enabling them to describe the load-deformation behavior of plates up to 64-plies thick for a wide range of support conditions.

In a separate study of damage mechanisms, Elber[3] identified the sequence in which damage occurs and measured the fiber damage near the bottom fibers. At the same time he showed that the damage mode, in actual impact tests at velocities around 5 m/s, was similar to the damage mode in the static tests. He postulated that the massive backface spalling, which often is the first visible sign of damage in laminates, is related to the low-peel/mode-fracture toughness in brittle resins and that it is trackable by static analysis.

Shivakumar et al.[4] analyzed the impact damage problem using the Ritz technique and large deflection theory for the circular plate problems treated in Refs. 1 and 2. The classical solutions presented in texts such as Timoshenko and Woinowsky-Krieger,[5] which use the Ritz technique, represent only a membrane correction to the plate stiffness. Further classical solutions[4,5] assume that the functional form of the deformed shape of the plate is identical to the functional form of the deformed shape of the plate determined by the small deflection solution. Because of this assumption, the functional form of the deformed shape of the plate and the radius of the points of inflection (radius at which curvature is zero) would be identical for all load levels. The functional form of the deformed shape of the plate and radius of the points of inflection, however, do change because at higher load levels the plate undergoes large deformations and the external load is partly equilibrated by the membrane action.

An accurate prediction of the deformed shapes is particularly useful in stress analyses, since stresses are proportional to the curvatures. The plate analysis based on the classical solution,[4,5] which assumes the functional form of the deformed shapes to be identical for all load levels, would incorrectly predict curvatures and, hence, would incorrectly predict stresses in the plate.

The objective of this study was, therefore, to develop a simple model to obtain the large deformation shapes and the load-displacement curves for thin plates under quasistatic point loads. The model does not have the constraining assumption that the deformed shape of the plate should be identical to the deformed shape determined by the small deflection plate solution. The simple model developed herein uses the plate and membrane solutions in conjunction with a coupling principle. In this model an analytically complete axisymmetric solution of a plate loaded centrally by a point load and along the radius by a distributive interactive load with the membrane is used. This solution does ignore the flexural anisotropy of the axially quasi-isotropic laminates analyzed. However, the experimental tests were performed to confirm that the flexural anisotropy is a secondary consideration and that the proposed analysis provides the desired results.

Analysis

In this section, a plate-membrane coupling model used to study the large deformation behavior of clamped, circular plates is presented first. Next, a numerical solution method to analyze these clamped, circular quasi-isotropic laminates under point load, using the plate-membrane coupling model, is presented.

Plate-Membrane Coupling Model

In the plate-membrane coupling model, two different plate problems are analyzed. First, a thin plate with shear and flexural stiffnesses, but no midplane extensional stiffness, is considered. The deflected shape of the plate under a point load is obtained using the classical small deformation theory. Second, a plate with midplane extensional stiffness but no shear and flexural stiffness, i.e., a membrane, is considered. The deformed plate shape obtained for the thin-plate problem is used in the membrane problem. For this deformed shape, membrane loads are calculated using a nonlinear membrane theory. Large deformation solutions of thin plates are then obtained by coupling these solutions of the plate and membrane problems. The details of the plate membrane coupling model are given below.

Consider a clamped, circular plate of thickness h and radius a, subjected to a central point load P as shown in Fig. 1. The plate was assumed to be a quasi-isotropic laminate of T300/5208 graphite/epoxy material with the stacking sequence $[45/0/-45/90]_s$ with material properties given in Table 1.

To analyze the large deformation behavior of this quasi-isotropic clamped circular plate, first a circular plate with a prescribed central deflection w_0 is considered. The objective of the analysis is to determine $w(r)$, the large deformation shape of the plate, and the central concentrated load P, given the prescribed w_0.

This problem, as mentioned earlier, can be decomposed into two component problems. Problem 1 is a plate with shear and flexural stiffnesses but no midplane extensional stiffness. Problem 2 is a plate with midplane extensional stiffness but no shear and flexural stiffnesses, i.e., a membrane.

In problem 1, the plate was assumed to be flexurally isotropic, even though a quasi-isotropic plate is anisotropic in flexure. This assumption was experimentally verified and will be discussed in detail later. The governing differential equation for axisymmetrical bending of a clamped, circular plate subjected to arbitrary axisymmetric loading and undergoing small deformations (see Ref. 5, Chap. 3, Sec. 15) is as follows:

$$\frac{d^3w}{dr^3}+\frac{1}{r}\frac{d^2w}{dr^2}-\frac{1}{r^2}\frac{dw}{dr}=\frac{Q(r)}{D_{eq}} \tag{1}$$

where $Q(r)$ is a shear force at any radius r and can be obtained as

$$Q(r)=\int_0^r p(\xi)\xi d\xi \Big/ r \tag{2}$$

where ξ is a dummy variable and $p(\xi)$ is the intensity of loading at any radius ξ. (See Fig. 2.)

In Eq. (1) D_{eq} is an equivalent flexural modulus for the quasi-isotropic laminate. The equivalent modulus D_{eq} can be obtained by equating bending energies of the quasi-isotropic laminates and an equivalent isotropic plate. A detailed derivation to determine the equivalent flexural modulus D_{eq} is presented in Appendix A. Equation (1) can be integrated numerically to obtain the deformed shape of the plate for a given intensity of the load $p(r)$.

In problem 2, a plate with midplane extensional stiffness but no shear and flexural stiffness, i.e., a membrane, is analyzed. As the quasi-isotropic laminates are axially isotropic, the governing differential equations for a clamped,

Table 1 Elastic properties of the plate

Material	Modulus, GPa E_{11}	E_{22}	G_{12}	Poisson's ratio
Gr/Ep lamina	131.0	13.0	6.4	0.34

Number of plies = 8
Laminate thickness = 1.05 mm
Stacking sequence: $[45/0/-45/90]_s$

N.B.: Subscripts 11 and 22 correspond to the longitudinal and transverse direction of fiber.

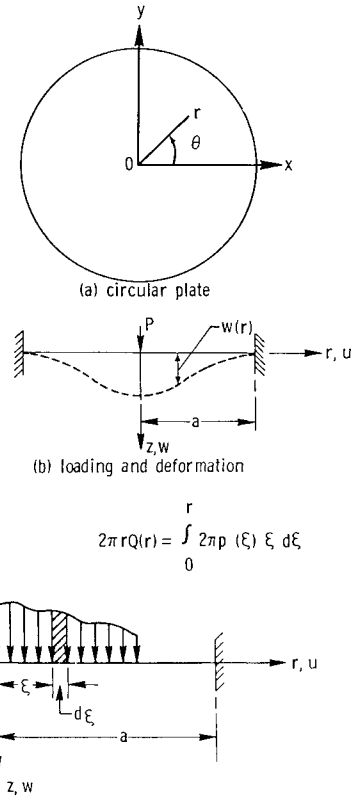

Fig. 1 Plate configuration.

Fig. 2 Arbitrarily axisymmetrically loaded circular plate.

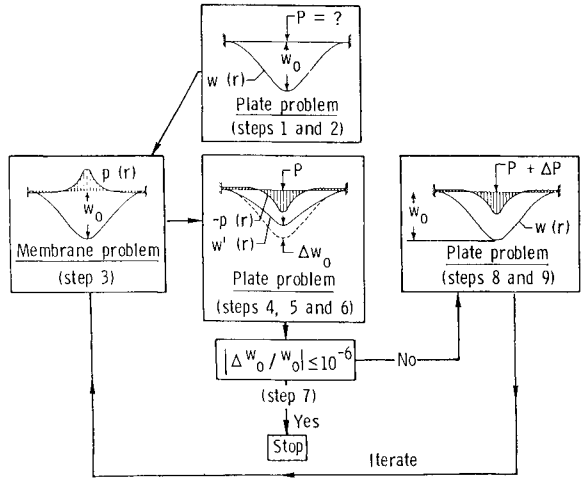

Fig. 3 Plate-membrane coupling model.

circular isotropic membrane are[6]

$$\frac{2r}{E}\left[3\frac{d\sigma_r}{dr}+r\frac{d^2\sigma_r}{dr^2}\right]+\left(\frac{dw}{dr}\right)^2=0 \tag{3}$$

$$\left(\frac{dw}{dr}\right)^2=\left[\int_0^r p(\xi)\xi d\xi \Big/ rh\sigma_r\right]^2 \tag{4}$$

where σ_r is the radial stress. If the displacement w is known, the rotation dw/dr is known and, hence, the radial stress σ_r can be determined by integrating Eq. (3). If the radial stress σ_r is known, the loading $p(r)$ on the membrane can be determined by using Eq. (4).

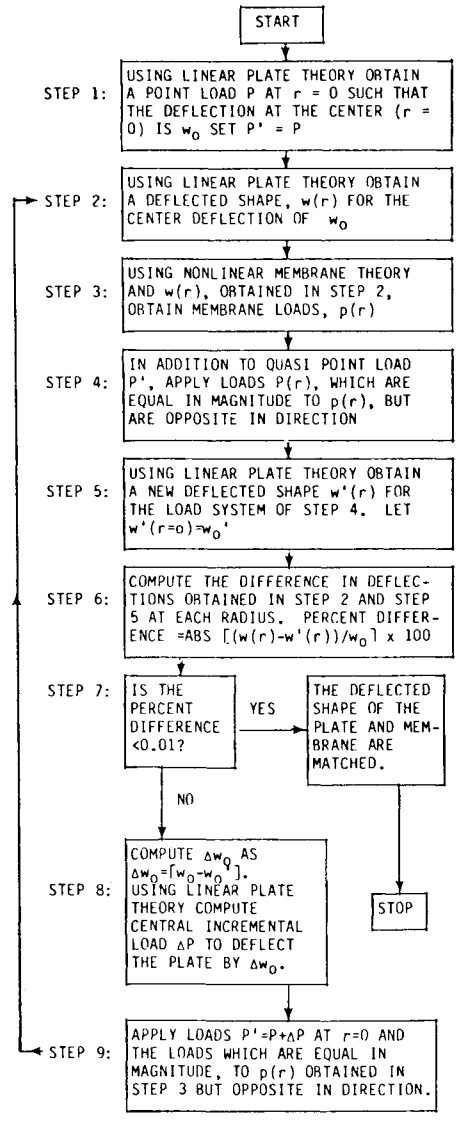

Fig. 4 Flow chart for the plate-membrane coupling model.

The large deformation solution for a quasi-isotropic clamped, circular laminate given the prescribed central point deflection w_0 can be obtained using the governing Eqs. (1–4) and the appropriate coupling of plate and membrane problems, as shown in the flow chart of Fig. 3. The procedure is further detailed in Fig. 4.

For a given prescribed central deflection w_0, the central point load P and the deformed shape $w(r)$ of a circular, clamped plate are calculated using Eq. (1) (steps 1 and 2 in Figs. 3 and 4). The loading $p(r)$, required in the membrane problem to produce the calculated thin plate deformed shape $w(r)$, is determined next, step 3. A loading equal in magnitude to $p(r)$, but of opposite sign, and the previously calculated point load P are then applied to the plate problem, step 4. A new deformed shape $w'(r)$ is calculated for the plate due to the combined loading $-p(r)+P$, step 5. The new displacement function $w'(r)$ is less than the original displacement $w(r)$ since the membrane loading $-p(r)$ acts in a direction opposite to P. Thus, the central deflection w_0 is reduced by an amount Δw_0 equal to $w_0 - w_0'$, step 6.

To produce the original central deflection w_0, an incremental load ΔP must be applied to the center of the plate. The magnitude of this incremental load is calculated from Eq. (1), step 8. Now the incremental load ΔP, the original point load P, and the negative membrane loading $-p(r)$ are applied to the thin plate problem, step 9. This loading

system will now yield a central deflection of w_0, the original value. However, the new deflected shape $w(r)$, due to the combined load of $\Delta P+P-p(r)$, will be different from the original shape. Thus, a revised membrane loading must be calculated using the new $w(r)$; this iteration process continues until the deflected shapes $w(r)$ obtained in any two consecutive iterations differ by less than some preset error factor, step 7.

Once the iterative process has converged, a central point load and the negative membrane load $-p(r)$ will be acting on the plate problem, while the membrane load $p(r)$ will be acting on the membrane problem. When these two solutions are coupled, the two membrane loads cancel each other, leaving only central point load P. (The coupled plate and the membrane are analogous to two coupled parallel springs, one with a linear plate stiffness and the other with a nonlinear membrane stiffness. Both springs undergo a deflection w_0 when an unknown load P is applied to the spring system. This unknown load P can be obtained by the addition of plate and membrane loads.) Thus it is possible to determine the large deflection shape of the plate and the magnitude of the central concentrated load, given a prescribed central deflection w_0.

Instead of prescribing a central deflection w_0, one could formulate the problem for a prescribed central point load P. The analysis procedure for this case is straightforward with minor differences and is as follows.

The problem, as before, is also decomposed into two component problems. By using the center point load P in the plate problem, the deflected shape $w(r)$ and the central deflection w_0 are obtained using Eq. (1). Then steps 2-6 (see Figs. 3 and 4) are repeated as earlier. Since, in step 4, the membrane load $p(r)$ is applied in the opposite direction, this again causes a reduction in central deflection w_0 (see step 6 in Fig. 4). At this stage, instead of incrementing the center point load P, new membrane loads $p(r)$ are calculated using the deformed shape $w'(r)$ obtained in step 5 (see step 3 in Fig. 4). This procedure is repeated until the deflected shapes obtained in any two consecutive iterations are almost identical.

A complete solution can now be obtained by coupling the plate-membrane solutions. When the final plate and membrane solutions are coupled as before, the $p(r)$ loads on the plate and membrane nullify each other and the original prescribed central point load is left on the plate. The corresponding matched central deflection w_0 and the deflection shape $w(r)$ are the large deformation solutions of the clamped, circular plate subjected to a prescribed central point load.

This procedure, although presented for a central concentrated load, can be applied in a similar manner to obtain the large deformation solutions for arbitrarily axisymmetrically loaded, clamped, circular plates. If, on the other hand, the large deformation shape of the plate is known, it can be used in the linear plate theory to calculate the plate loads, and in the nonlinear membrane theory to calculate the membrane loads. The sum of these two loads gives the complete large deformation solution.

Solution Method

To solve the governing equation (1) for the deflection w, the ordinary differential equation (1) was replaced by a set of linear algebraic equations using difference quotients. These linear algebraic equations were solved numerically to obtain rotations and displacements. The nonlinear governing equations (2) and (3) were replaced by a set of nonlinear algebraic equations using difference quotients. These nonlinear equations were solved, using a technique developed in Ref. 6, to obtain the membrane loads. Details of the solution method for component problems 1 and 2 (plate and membrane) are given subsequently.

Problem 1, plate solution. The circular plate domain was discretized into m regions and $(m+1)$ nodes. The nodes were numbered from the center of the plate toward the clamped end. Denoting $w(n)$ as the transverse displacement at the nth node, the governing equation (1) at any node n is

$$\frac{d^3w(n)}{dr^3}+\frac{1}{r_n}\frac{d^2w(n)}{dr^2}-\frac{1}{r_n^2}\frac{dw(n)}{dr}=\int_0^{r_n}p(\xi)\xi d\xi\Big/r_nD_{eq} \quad (5)$$

The integral in the above equation is replaced by a summation and Eq. (5) is rewritten as

$$\frac{d^3w(n)}{dr^3}+\frac{1}{r_n}\frac{d^2w(n)}{dr^2}-\frac{1}{r_n^2}\frac{dw(n)}{dr}=\sum_{i=1}^{n}\frac{p_i(r_i^2-r_{i-1}^2)}{2r_nD_{eq}} \quad (6)$$

where p_i is the intensity of the load over the ith region $r_{i-1}\le r\le r_i$. First, second, and third derivatives of the displacements in the governing equation (6) were replaced by standard difference quotients.[7]

For the circular quasi-isotropic laminate with axisymmetric load, the boundary conditions are as follows:

1) The transverse displacement w at the fixed edge $(r=a)$ is equal to zero.

2) Both the rotations (dw/dr) at the center $(r=0)$ and at the fixed edge $(r=a)$ are equal to zero.

Using the governing equation (6) and the two boundary conditions in the form of finite difference quotients, $(m+1)$ linear algebraic equations were obtained. These algebraic equations contained $(m+1)$ unknowns, viz., $w(1),w(2),\ldots,w(m+1)$. These $(m+1)$ equations were solved simultaneously to obtain the transverse displacement at each node.

Problem 2, membrane solution. The solution domain was discretized into the same number of axisymmetric regions and nodes as for the plate. As in Ref. 6, denoting $\sigma_r(n)$ and $(dw/dr)/n$ as the radial stress and rotation at the nth node, respectively, Eqs. (3) and (4) become

$$2\frac{r_n}{E}\left[3\frac{d\sigma_r(n)}{dr}+r_n\frac{d^2\sigma_r(n)}{dr^2}\right]+\left[\frac{dw(n)}{dr}\right]^2=0 \quad (7)$$

$$\frac{1}{2}\left(\frac{dw(n)}{dr}\right)^2=\frac{1}{8}\left[\frac{1}{r_nh\sigma_r(n)}\sum_{i=1}^{n}p_i(r_i^2-r_{i-1}^2)\right]^2 \quad (8)$$

First and second derivatives of the radial stress in the governing equations (7) and (8) were replaced by standard difference quotients. For the circular membrane with ax-

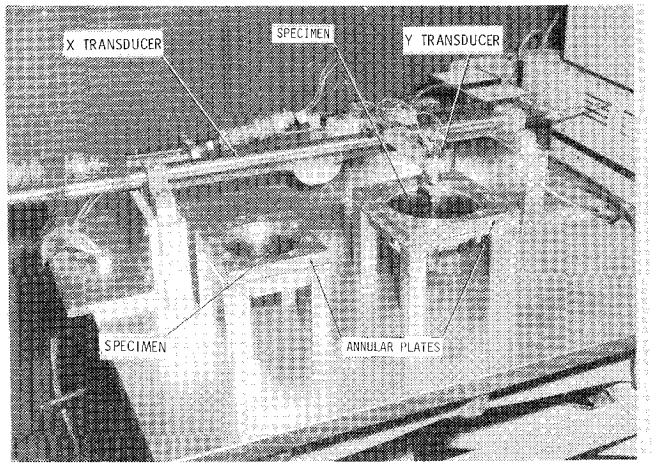

Fig. 5 Experimental setup.

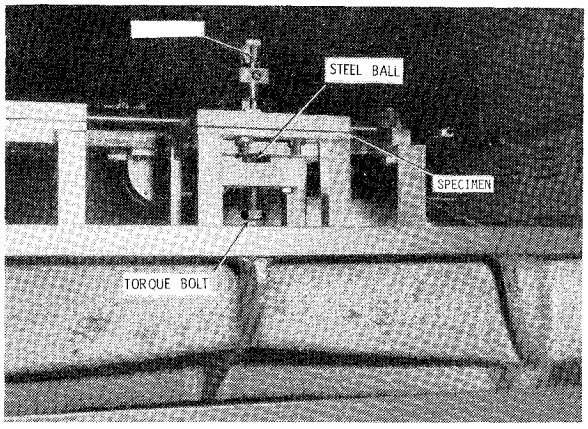

Fig. 6 Loading on the specimen.

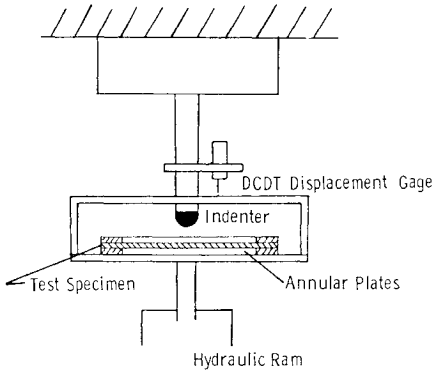

Fig. 7 Static loading on the quasi-isotropic circular laminate.

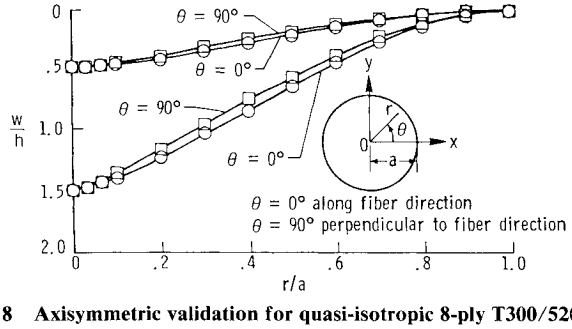

Fig. 8 Axisymmetric validation for quasi-isotropic 8-ply T300/5208 laminate.

isymmetric loading, boundary conditions are given below:

1) Both the radial displacement u and the transverse displacement w at the fixed edge ($r=a$) are equal to zero.

2) The radial displacement u and the rotation (dw/dr) at the center ($r=0$) are equal to zero.

By using the procedure described in Ref. 6, these boundary conditions were transformed in terms of the radial stresses, and the nonlinear governing equations (7) and (8) were solved numerically using Newton-Raphson's method in conjunction with the finite-difference method.

With these plate and membrane solutions in conjunction with the plate-membrane coupling model discussed before, the large deformation shapes and the load-displacement curves for the clamped, circular quasi-isotropic laminates were obtained.

Experimental Procedure

Circular, quasi-isotropic graphite/epoxy laminates with the stacking sequence of $[45/0\text{-}45/90]_s$ were tested. The plate thickness was 1.05 mm for all specimens.

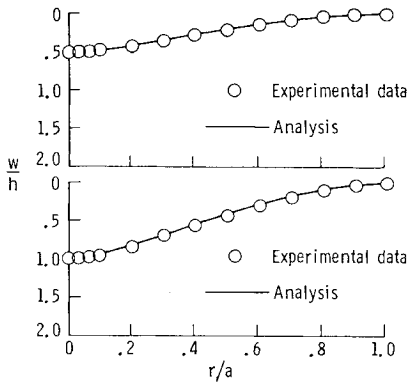

Fig. 9 Deflected shapes for the laminate under quasi-isotropic point loads for $w_0/h=0.5$ and 1.0.

Circular laminates with 76.2 mm (3 in.) or 101.6 mm (4 in.) diam were bolted between two annular plates as shown in Fig. 5. These steel plates provided clamped boundary conditions for the specimens. A torque bolt arrangement was used to push a 25.4 mm diam steel ball against the laminate and provide the desired static loading (see Fig. 6).

A transversing horizontal direct current differential transducer (DCDT) and a vertical DCDT were used to measure the deflected shapes of the clamped, circular quasi-isotropic laminates as shown in Fig. 5. An x-y plotter was attached to the horizontal and vertical transducers to plot the deflected shapes of the quasi-isotropic laminates. The vertical DCDT observations were recorded for 76.2 mm and 101.6 diam plates at intervals of 2.54 mm along three diametrical lines of the clamped, circular quasi-isotropic laminates.

The first set of observations were made along the fiber direction ($\theta=0$ deg) of the eighth ply (farthermost ply from the point of load application). The second and third set of observations were made on a line perpendicular ($\theta=90$ deg) and on a line 45 deg ($\theta=45$ deg) to the fiber direction of the eighth ply. These three sets of observations were recorded for central deflection-to-plate-thickness ratios (w_0/h) of 0.5, 1.0, 1.5, and 2.0.

To obtain the load-deflection curves, the static loading tests were conducted in a servohydraulic testing machine. The test specimens were clamped to a platform, shown in Fig. 7, which was mounted on the hydraulic ram, and load was applied to the center of the specimen by means of a punch, tipped with a 25.4 mm diam steel ball. A DCDT displacement gage was attached to the indenter to measure plate deflection as the load was applied. The electric signals from the load cell and the displacement gage were given as input to the x-y plotter to allow direct load-displacement plotting.

Results and Discussion

In this section, first the validity of flexural isotropy in circular quasi-isotropic laminate is discussed. Then the results of the plate-membrane coupling model for clamped, circular quasi-isotropic laminates subjected to point loads are presented. Lastly, the movement of radius of point of inflection (the radius at which curvatures are zero) with the change in the central deflection of the laminate is compared with the classical plate solution.[5]

To verify the flexural isotropy in circular quasi-isotropic laminates, experimental measurements were made along three diametrical lines at $\theta=0$, 45, and 90 deg for values of w_0/h ranging from 0.5 to 2.0. Figure 8 presents the typical deflected shapes for w_0/h ratios of 0.5 and 1.5. The deflected shapes for w_0/h ratios of 1 and 2 showed similar trends. The experimental observations showed that the deflected shapes along $\theta=0$ and $\theta=90$ deg are nearly iden-

tical. The deflected shapes along $\theta = 45$ deg were bounded by the shapes along $\theta = 0$ deg and $\theta = 90$ deg. The maximum differences between the $\theta = 0$ and 90 deg observations occurred near $r/a = 0.4$ and were between 6–7% of the maximum center deflections. Thus, the experimental observations indicated that clamped, circular quasi-isotropic laminates subjected to axisymmetric loading behave as if they are almost flexurally isotropic and have nearly axisymmetric bending behavior.

For the purpose of analysis, the region $0 < r < a$ was divided into 60 axisymmetric elements; 60 elements were found to be sufficient for the convergence of the displacement solutions in the case of membrane and plate problems.

From the plate-membrane coupling model it was observed that as plate central deflection-to-plate-thickness ratio (w_0/h) increases, the number of iterations required to match the deflected plate and membrane shapes increases. Table 2 presents the number of iterations required to obtain the large deformation shapes of the clamped, circular quasi-isotropic laminates under point loads for w_0/h ratios ranging from 0.5 to 2.0.

Figures 9 and 10 present the measured deflected shapes at $\theta = 0$ deg and the analytical deflected shapes obtained with the plate-membrane coupling model, for w_0/h ratios ranging from 0.5 to 2.0. Excellent agreement is observed between experimental and analytical results.

The deflected shapes obtained using the plate-membrane coupling model were compared with the deflected shapes obtained using the classical solution.[5] Figure 11 presents the percentage errors in the deflected shape of the classical solution, relative to the present solution, at various radii for w_0/h ratio of 2.0. It is observed that the maximum error is about 4% and occurs at the radius of the point of inflection ($r/a = 0.233$). Since stresses are proportional to curvatures, even small relative errors in curvatures may result in significant errors in stress predictions in the plate undergoing large deformation.

Figure 12 presents the comparison of measured load-displacement curve and the analytical load-displacement curve obtained using the plate-membrane coupling model. The analytical results were found to be within 6% of the experimental results. The differences between the analytical and experimental results are probably due to experimental errors which might have been introduced while practically simulating the clamped boundary conditions.

Figure 13 presents the movement of the point of inflection with the change in the central deflection-to-plate-thickness ratios (w_0/h). As pointed out in the introduction, the classical solution[5] has the constraining assumption that the functional form of the deformed shape is identical for all w_0/h ratios, hence, the point of inflection shows no movement with the change in the w_0/h ratios and is shown as a horizontal line in Fig. 13. This point of inflection is located at $r/a = 0.3678$ (see Appendix B). The plate-membrane coupling model, on the other hand, does not make any assumption on the deformed shape of the plate and, hence, on the point of inflection. The deformed shape and the point of inflection are obtained as a part of the solution. The symbols in Fig. 13 show the position of the point of inflection for different values of w_0/h. For increasing central deflection the point of inflection moves toward the center of the plate

Table 2 Number of iterations required for solution

Plate center deflection-to-thickness ratio, w_0/h	No. of iterations
0.5	9
1.0	11
1.5	14
2.0	21

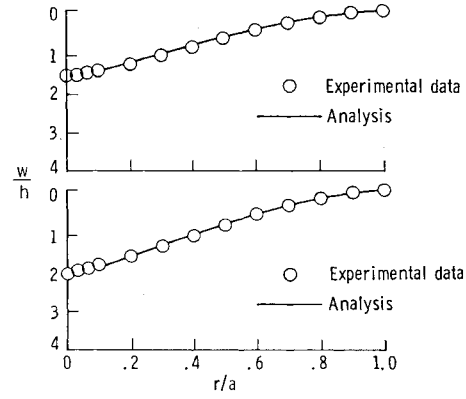

Fig. 10 Deflected shapes for the laminate under quasistatic point loads for $w_0/h = 1.5$ and 2.0.

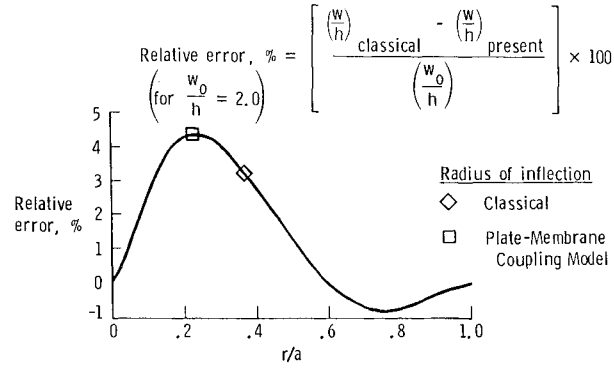

Fig. 11 Percentage errors in the classical solution relative to the present solution.

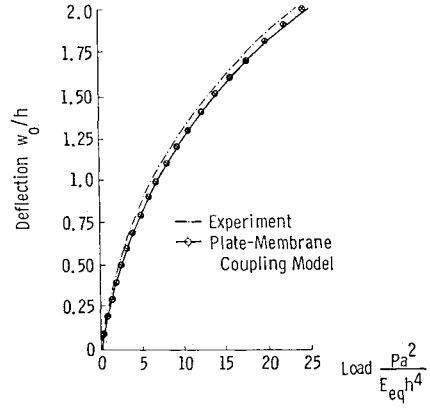

Fig. 12 Comparison of experimental and plate-membrane coupling model load-displacement curves.

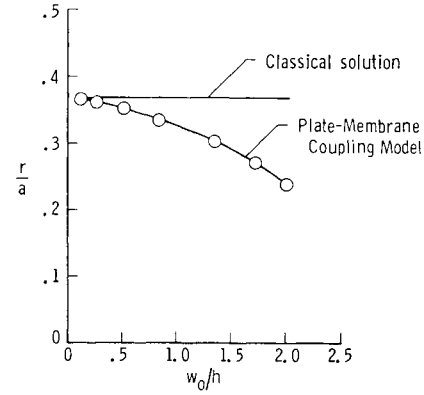

Fig. 13 Movement of radius of inflection as a function of center deflection.

($r=0$). The inward movement of the point of inflection with increasing w_0/h occurs, since, as w_0/h increases, the plate behaves more like a membrane than a flexural plate. That is, as w_0/h increases, the external load is equilibrated more and more in membrane action rather than in flexural action.

Conclusions

Eight-ply T300/5208 quasi-isotropic composite plates were analyzed to study the large deformation behavior under low-velocity impact-type point loads. A simple plate-membrane coupling model was formulated and solved numerically. Experiments were undertaken on the quasi-isotropic circular, clamped laminates. For experimental and analytical purposes, the impact-type point loads were replaced by equivalent quasistatic loads. The study resulted in the following conclusions:

1) The large deflection behavior of thin circular composite plates can be obtained using a simple plate-membrane coupling model.

2) The functional form of the deformed shape of the plate undergoing large deformations is different from the small deflection plate solution in that the deformed shape is a function of the center point displacements and, thus, is different for different load levels. Furthermore, for a plate undergoing large deformations, there is an inward movement of the radii of points of inflection.

3) Although the circular quasi-isotropic plates are flexurally anisotropic, the anisotropy usually is small and, hence, the quasi-isotropic plates were analyzed by replacing anisotropic bending stiffness components with the equivalent flexural stiffnesses for isotropic plates.

Appendix A: Equivalent Flexural Modulus

Laminate extensional, coupling, and bending stiffnesses were calculated using classical laminated plate theory[8] for a $[45/0/-45/90]_s$ quasi-isotropic laminate with the elastic properties given in Table 1. The extensional stiffness is independent of the polar angle θ (see Fig. 1) and is constant over the entire plate domain. This indicates that the laminate behaves perfectly isotropic for membrane and inplane loadings.

Since the laminate is symmetric, the coefficients of the coupling stiffness are found to be zero. The laminate bending stiffness depends on θ. However, an equivalent bending stiffness that is independent of θ can be determined by equating the flexural strain energies of the clamped, circular quasi-isotropic laminate and an equivalent circular isotropic plate.

For a clamped, circular quasi-isotropic laminate, the total strain energy in bending is

$$U_b=\frac{1}{2}\int_0^{2\pi}\int_0^{a}\{M\}^T\{\kappa\}r\,dr\,d\theta \tag{A1}$$

where

$$\{M\}=\begin{Bmatrix}M_r\\M_\theta\\M_{r\theta}\end{Bmatrix}\qquad\{\kappa\}=\begin{Bmatrix}\kappa_r\\\kappa_\theta\\\kappa_{r\theta}\end{Bmatrix} \tag{A2}$$

M_r, M_θ, and $M_{r\theta}$ are the moments and κ_r, κ_θ, and $\kappa_{r\theta}$ are the corresponding curvatures. For the quasi-isotropic circular laminate, the moments and curvatures are related as

$$\{M\}=[D]\{\kappa\} \tag{A3}$$

where

$$[D]=\begin{bmatrix}D_{11}&D_{12}&D_{16}\\D_{12}&D_{22}&D_{26}\\D_{16}&D_{26}&D_{66}\end{bmatrix} \tag{A4}$$

Substitution of Eq. (A3) into Eq. (A1) yields

$$U_b=\frac{1}{2}\int_0^{2\pi}\int_0^{a}\{\kappa\}^T[D]\{\kappa\}r\,dr\,d\theta \tag{A5}$$

Equation (A5) can be expanded as

$$U_b=\frac{1}{2}\int_0^{a}\int_0^{2\pi}[\kappa_r^2D_{11}+2\kappa_r\kappa_\theta D_{12}+2\kappa_r\kappa_{r\theta}D_{16}+2\kappa_{r\theta}\kappa_\theta D_{26}+\kappa_\theta^2D_{22}+\kappa_{r\theta}^2D_{66}]\,r\,dr\,d\theta \tag{A6}$$

The coefficients D_{11}, D_{12}, D_{16}, D_{26}, and D_{66} in Eq. (A6) are all known functions of θ (see Ref. 8). If one asumes that the curvatures are functions of r alone, then the integrations over θ in Eq. (A6) can be carried out and Eq. (A6) can be written as

$$U_b=\frac{2\pi}{2}\int_0^{a}[\kappa_r^2D'_{11}+2\kappa_r\kappa_\theta D'_{12}+2\kappa_r\kappa_{r\theta}D'_{16}+2\kappa_{r\theta}\kappa_\theta D'_{26}+\kappa_\theta^2D'_{22}+\kappa_{r\theta}^2D'_{66}]\,r\,dr \tag{A7}$$

where

$$D'_{ij}=\frac{1}{2\pi}\int_0^{2\pi}D_{ij}\,d\theta,\quad i,j=1,\ 2,\ \text{and}\ 6$$

The bending energy of an isotropic plate with a flexural modulus D_{eq}, a Poisson's ratio of ν_{eq}, and curvatures κ_r, κ_θ, $\kappa_{r\theta}$ (the same as that of the quasi-isotropic laminate) can be written as

$$U_b\ (\text{isotropic plate})=\frac{1}{2}\int_0^{a}\int_0^{2\pi}\left[\kappa_r^2D_{eq}+2\kappa_r\kappa_\theta\nu_{eq}D_{eq}+\kappa_\theta^2D_{eq}+\kappa_{r\theta}^2\left(\frac{1-\nu_{eq}}{2}\right)D_{eq}\right]r\,dr\,d\theta \tag{A8}$$

The flexural modulus D_{eq} and the Poisson's ratio ν_{eq} are independent of θ, hence, integrations on θ can be carried out and Eq. (A8) can be written as

$$U_b\ (\text{isotropic plate})=\frac{2\pi}{2}\int_0^{a}\left[\kappa_r^2D_{eq}+2\kappa_r\kappa_\theta\nu_{eq}D_{eq}+\kappa_\theta^2D_{eq}+\kappa_{r\theta}^2\left(\frac{1-\nu_{eq}}{2}\right)D_{eq}\right]r\,dr \tag{A9}$$

For the same arbitrary curvatures κ_r, κ_θ, $\kappa_{r\theta}$ on the composite laminate and the isotropic plate, the bending strain energies must be the same because of the assumed energy equivalence. Hence, comparing curvature coefficients of Eqs. (A7) and (A9), equivalent bending stiffness D_{eq} and Poisson's ratio ν_{eq} can be determined as

$$D_{eq}=\frac{1}{2\pi}\int_0^{2\pi}D_{11}\,d\theta \tag{A10}$$

$$\nu_{eq}D_{eq}=\frac{1}{2\pi}\int_0^{2\pi}D_{12}\,d\theta \tag{A11}$$

$$D_{eq}=\frac{1}{2\pi}\int_0^{2\pi}D_{22}\,d\theta \tag{A12}$$

$$\left(\frac{1-\nu_{eq}}{2}\right)D_{eq}=\frac{1}{2\pi}\int_0^{2\pi}D_{66}\,d\theta \tag{A13}$$

If circular quasi-isotropic laminates were flexurally isotropic, then the integrals

$$\frac{1}{2\pi}\int_0^{2\pi} D_{16}\mathrm{d}\theta \quad \text{and} \quad \frac{1}{2\pi}\int_0^{2\pi} D_{26}\mathrm{d}\theta \tag{A14}$$

would be equal to zero. However, in the circular quasi-isotropic laminate under consideration, the integrals in Eq. (A14) were nonzero. The integrals were found to be about 2.5% of $1/2\pi\int_0^{2\pi} D_{11}\mathrm{d}\theta$ and hence were neglected in this analysis.

Equations (A10–A13) represent four equations with two unknowns, D_{eq} and ν_{eq}. The first two equations, (A10) and (A11), are sufficient to evaluate the two unknowns D_{eq} and ν_{eq}. Equation (A12), because of symmetries, is essentially the same as Eq. (A10). For the material properties in Table 1, the values of D_{eq} and ν_{eq} were found to be 5.688 and 0.31 N-m, respectively. The values of D_{eq} and ν_{eq}, when substituted into the last equation (A13), satisfied that equation exactly.

For the lamina properties in Table 1, the value of equivalent Young's modulus E_{eq} was obtained from the equivalent flexural modulus D_{eq} as

$$E_{eq} = D_{eq}\cdot 12\cdot(1-\nu_{eq}^2)/h^3 \tag{A15}$$

and was found to be 53.3 GPa.

This value of E_{eq} is exactly the same as the inplane Young's modulus of the laminate obtained using the ply properties in Table 1 and the classical laminate theory.

Appendix B: Radius of Point of Inflection

The classical large deformation theory[4,5] assumes the deformation shape of a clamped circular plate under central point load as

$$w(r) = w_0\left[1-\frac{r^2}{a^2}+2\,\frac{r^2}{a^2}\,\ell n\,\frac{r}{a}\right] \tag{B1}$$

Furthermore, the classical theory assumes that the functional form of the deformation shape remains unchanged for various values of central deflection w_0. Thus the radius of the point of inflection (the radius at which curvature is zero) is independent of w_0/h. The radius of the point of inflection can be obtained as follows. By differentiating Eq. (B1) twice, curvature can be written as

$$\frac{\mathrm{d}^2 w}{\mathrm{d}r^2} = \frac{4w_0}{a^2}\left[1+\ell n\,\frac{r}{a}\right] \tag{B2}$$

The radius of the point of inflection is the radius at which $(\mathrm{d}^2 w/\mathrm{d}r^2)=0$. Hence,

$$\frac{4w_0}{a^2}\left[1+\ell n\left(\frac{r}{a}\right)\right]=0 \tag{B3}$$

yields the radius of point of inflection as

$$(r/a) = e^{-1} = 0.3678 \tag{B4}$$

References

[1]Llorens, R. E. and Gause, L. W., "Low Velocity, Transverse Normal Impact on a Clamped Plate," NADC-81250-60, Oct. 1981.

[2]Bostaph, G. M. and Elber, W., "Static Indentation on Composite Plates for Impact Susceptibility Evaluation," *Army Symposium on Solid Mechanics*, Cape Cod, MA, 1982, pp. 288–317.

[3]Elber, W., "Failure Mechanics in Low-Velocity Impacts on Thin Composite Plates," NASA TP 2152, 1983.

[4]Shivakumar, K. N., Elber, W., and Illg, W., "Prediction of Low-Velocity Impact Damage in Thin Circular Laminates," *AIAA Journal*, Vol. 23, March 1985, pp. 442–449.

[5]Timoshenko, S. and Woinowsky-Krieger, S., *Theory of Plates and Shells*, McGraw-Hill, New York, 1959.

[6]Kelkar, A., Elber, W., and Raju, I. S., "Large Deflections of Circular Isotropic Membranes Subjected to Arbitrary Axisymmetric Loading," *Computers and Structures*, Vol. 21, No. 3, 1985, pp. 413–421.

[7]Scarborough, J. B., *Numerical Mathematical Analysis*, The Johns Hopkins Press, Baltimore, MD, 1966.

[8]Jones, R. M., *Mechanics of Composite Materials*, McGraw-Hill, New York, 1975.